This article has been accepted for publication in a future issue of this journal, but has not been fully edited. Content may change prior to final publication. Citation information: DOI10.1109/TAP.2023.3335840, IEEE Transactions on Antennas and Propagation

Spoof Surface Plasmon Polaritons Based Antenna and Array by Exciting both Even and Odd Mode Resonances

Lehu Wen, Wei Hu, *Senior Member, IEEE,* Bo Pang,
Qi Luo, *Senior Member, IEEE*, and Steven Gao, *Fellow, IEEE*,

***Abstract*—Spoof surface plasmon polaritons (SSPPs) based antenna and array by exciting both even and odd mode resonances are developed and investigated in this paper. Different from others' work and for the first time, we use the separated corrugated grooves to achieve the consistent fundamental even and odd mode resonances on the same SSPPs aperture. In this way, the even and odd mode resonances can be operated in the same frequency band. Also for the first time, we introduce the SSPPs into an orthogonal-mode resonated antenna pursuing high isolated radiation. New challenges including the feed methods and impedance matching of two different resonant modes are overcome by introducing the capacitive patch and triangular cuts on the SSPPs. Finally, the SSPPs antenna and array were tested for performance investigation. It is found that in addition to the obtained wide overlapped impedance bandwidth of 14.8%, a very high isolation of 29 dB is achieved in the developed compact antenna element. The couplings between other antenna elements, radiation patterns, gains, and efficiencies of the array are also investigated. Both the measured and simulated results show that SSPPs and the developed antenna can be very appealing in MIMO applications owing to their orthogonal even-odd modes and compact structures.**

***Index Terms*—Even-mode resonance, odd-mode resonance, spoof surface plasmon polaritons.**

I. Introduction

As a special kind of electromagnetic wave, spoof surface plasmon polariton (SSPP) has been widely researched for wireless communication systems [1]. By drilling holes or etching grooves, SSPPs surface wave can be successfully excited, bounded, and propagated along the metal structure. It has the features of strong field confinement, decreased guided wavelength, and nonlinear dispersion diagram [2]. Especially, the highly confined dispersion properties of the SSPPs show that they can be utilized for the design of the compact-size and broadband passive and active devices for different communication systems.

SSPPs are the efficient and low-loss structures for electromagnetic wave transmissions, and the SSPPs wave can be transmitted mainly through two different modes, either even-mode or odd-mode. They are widely used for realizing different microwave components. Basically, SSPPs are researched for designing low-profile and broadband transmission waveguide devices [3]-[6]. Using the periodically corrugated grooves under odd mode excitation [4], low insertion loss transmission of less than 2 dB is realized in the 200 GHz band. SSPPs based power dividers [7]-[8], couplers [9], and detectors [10] are also investigated using this new type of transmission lines. In [7], an even-mode excited ultrawideband three-way power divider is developed by using periodically decorated metal and dielectric, which operates in the frequency band of 3.0-11.8 GHz. Based on the Pancharatnam Berry metasurface and diodes, direction controllable SSPPs coupler is obtained in [9]. Using SSPPs structure, the detector [10] can have 90% improvement of the detection sensitivity over the low input RF power. As one of the metasurface unit cells, SSPPs can also be used to designing meta-coupler [11], frequency selective surface [12], and lens [13]. By properly allocating non-resonant regions and resonant regions on a zone plate, a high-Q lens is constructed in [13] with thermally controlled selective and focusing behaviour.

In addition to the above passive devices, antennas based on SSPPs are also widely investigated [14]-[20]. By properly modulating SSPP unit cell, the bounded surface wave is successfully excited for radiation [14]-[16]. In [15], two different periods are modulated on the even-mode excited SSPPs, and two beams radiate in both forward and backward directions for the designed leaky wave antenna. To get a unidirectional radiation, fixed endfire radiated antennas are developed [17]-[18]. By using the microstrip-to-slotline converter [18], the odd-mode radiation of the SSPPs is excited with a stable endfire radiation covering a wide bandwidth of 2.4-5 GHz. In [19], by designing the SSPPs into a polarizer, and a dual circularly polarized horn antenna is realized with a wide axial ratio bandwidth of 26%. Recently, multiple-input multiple-output (MIMO) technology has aroused researchers' great interests owing to its advantage of using multiple antennas to increase the system throughput for multiple users

This work was supported by Engineering and Physical Sciences Research Council under Grant EP/N032497/1, Grant EP/P015840/1, and Grant EP/S005625/1. *(Corresponding author: Lehu Wen.)*

L. Wen is with the Department of Electronic and Electrical Engineering, Brunel University London, Uxbridge, UB8 3PH, U.K. (Email: LehuWen@ieee.org)

W. Hu and B. Pang are with the National Key Laboratory of Antennas and Microwave Technology, Xidian University, Xian, 710071, China.

Q. Luo is with the School of Physics, Engineering and Computer Science, University of Hertfordshire, Hatfield, AL10 9AB, UK.

S. Gao is with the Department of Electronic Engineering, the Chinese University of Hong Kong, 999077, Hong Kong.

[21]. To achieve the low correlated and high isolated multi-path signals for MIMO applications, orthogonal radiations are utilized in the antennas design [22]-[26]. In [22]-[23], dual-polarized patch mode is used for unidirectional radiation. In [24]-[26], different orthogonal modes, such as the slot mode, loop mode, characteristic modes, differential mode, common mode, etc., are used for designing high isolated MIMO array antennas.

In this work, for the first time, both the even-mode and odd-mode radiations are successfully excited and simultaneously utilized on the same SSPPs aperture with a wide overlapped bandwidth and high isolation for MIMO applications. First, different from others' work, new corrugated grooves with a dedicated separate distance are developed aiming to achieve the consistent even and odd mode resonances on SSPPs. So that the same or very close resonant frequencies can be achieved for these two different modes on the same SSPPs structure. Then, based on this SSPPs structure, both the antenna element and array are developed for MIMO applications. In the antenna design, we use different methods, the capacitive patch and the triangular cuts, to overcome the impedance matching problems firstly encountered in the even and odd mode radiations in SSPPs. Finally, the MIMO array antenna was designed, fabricated, and measured for performance verification. Owing to the innate orthogonality of even-odd modes on SSPPs, very high isolation of better than 29 dB is achieved between two driven ports in the antenna element. In addition, benefiting from the introduced impedance matching methods, a wide overlapped impedance bandwidth of 3.31-3.84 GHz (14.8%) is obtained. The other performances, such as the couplings between other elements, radiation patterns, gain, efficiencies, etc., are also investigated for MIMO applications.

II. Even-Odd Mode of the SSPP Unit Cell

In this section, planar SSPPs are developed and discussed for the consistent even-odd mode resonances.

A. Consistency of Even-Odd Mode

It is known that the fundamental even and odd modes will transmit on the SSPPs. However the two modes have the different phase constants as they transmit on the same SSPPs. This denotes that at a given resonant length, the resonant frequencies of the even-mode and odd mode will be different. This will be undesirable when we use the SSPPs as the orthogonal resonators and want the same or similar working bandwidths of the two modes.

In this work, two SSPP unit cells are compared and selected aiming for a consistent transmission phase in both two modes at the same given length. As shown in Fig. 1, unit cell 1 is commonly selected as the SSPP unit cell for the guided wave transmission. It is composed of double-sided corrugated metallic grooves. Unit cell 2 is the type what we will use in this work, which is also double-sided with corrugated grooves, but the entire structure is split into two separate pieces at the center with a dedicated separate distance of d1.

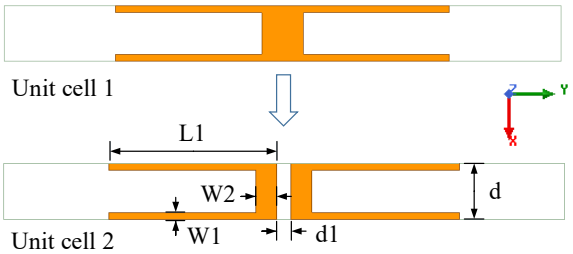

Fig. 1. SSPP unit cells with different configuration. (Parameters in the unit cell: L1=15 mm, W1=0.5 mm, d=4 mm, W2=1.5 mm, d1=0.5 mm.)

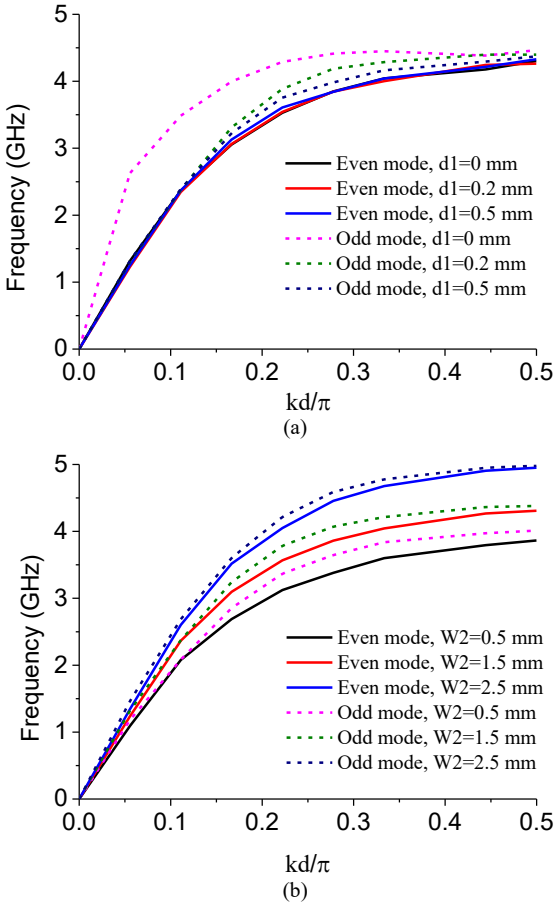

Fig. 2. Dispersion curve of the unit cell 2 varies with (a) different split distances d1 and (b) different widths W2.

Fig. 2 shows the dispersion characteristic of the two unit cells. First, let us look at the dispersion curves changing with different split distances (d1) in Fig 2 (a). Note that when d1 reduces to 0, the unit cell 2 will be degenerated into unit cell 1. For unit cell 1 or d1=0, we can find the dispersion curves of two fundamental modes are far away from each other as the designs in [27]-[28]. This means that at a given working frequency, the even and odd mode waves transmitted through the same unit cell will have a large phase difference. This is quite undesirable if we want a same resonant frequency using a same transmission length. When we split the structure with the distance, it is can be observed that phase constants of two different modes are getting closer as the distance increases from 0mm to 0.5mm. Fig. 2 (b) shows the dispersion curve changing with different width of the center metal (W2). It can be found that by increasing the width of the center metal, the phase

constants of two modes can be also getting closer. These two parametrical studies show that we can change the split distance and the width of the center metal to make the SSPP structure have the same or very close resonant frequencies.

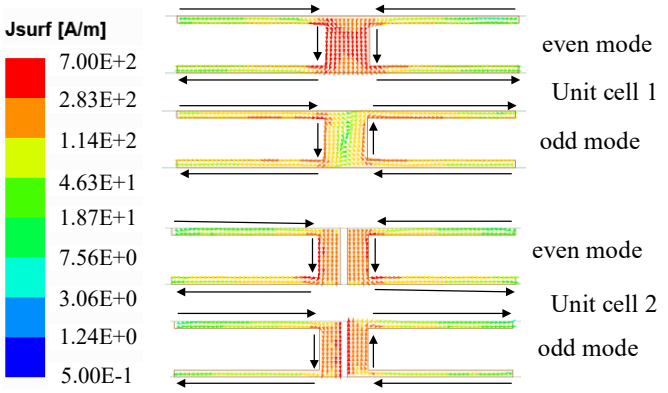

Fig. 3. Current distributions of the unit cell 1 and unit cell 2 at different even-odd resonant modes.

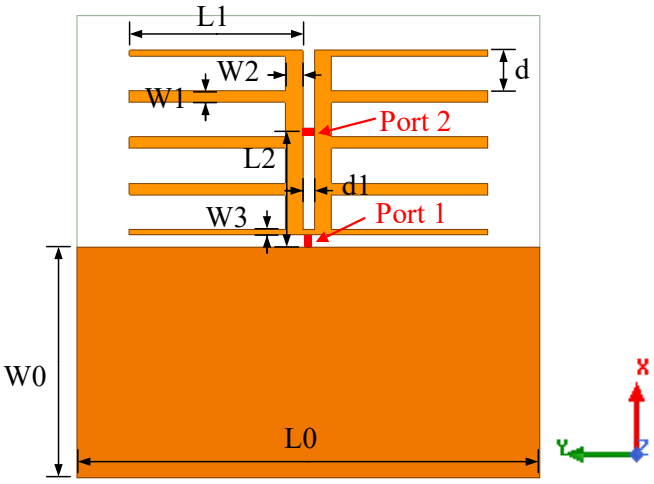

Fig. 4. Configuration of planar even-odd mode excited SSPPs. (Parameters detail, W0=20 mm, L0=40 mm, d=4 mm, L1=15 mm, W1=1 mm, L2=10 mm, W2=1.5 mm, d1= 0.5mm, W3= 0.5mm.)

To further illustrate the working principle of the different dispersion characteristics in these two unit cells, Fig. 3 shows the current distributions of the two unit cells under different even and odd mode resonances. As can be seen, the even-mode current distributions on the two unit cells are very similar, so that the split on the center metal has nearly no effect on the resonance of the even-mode resonance. However, the odd-mode current distributions on the two unit cells are different, especially at the center of the structures. It can be seen in unit cell 1, the current of unit cell 1 at the center becomes weak due to the inverse continuous currents on a same metal. Whereas for unit cell 2, the currents are evenly distributed on two separate vertical metals with inverse direction and strong magnitude due to the strong edge coupling effect. Because of the center split, the even-mode current magnitude distribution and odd-mode current magnitude distribution on the two separate metals of unit cell 2 are very similar, except their inverse current directions on the right part. Therefore, unit cell 2 can have very close even-mode and odd-mode resonance frequencies at the same structure.

B. Planar Even-Odd mode Excited SSPPs

Based on the discussed SSPP unit cell, a model of planar even-odd mode excited SSPPs is studied and shown in Fig. 4 to further illustrate the consistent even-mode and odd-mode resonances. As shown in Fig. 4, this model is composed of four SSPP unit cells. The unit cell has the same configuration as the developed SSPP unit cell 2. To conveniently excite the even-mode resonance, a lumped port 1 is inserted between a rectangular ground and the SSPPs. Note that a narrow center strip is introduced to connect the two separate metals for the convenience of the even-mode excitation. Another lumped port 2 is inserted in the split to excite the odd-mode resonance with the feed distance of L2 to the ground plane.

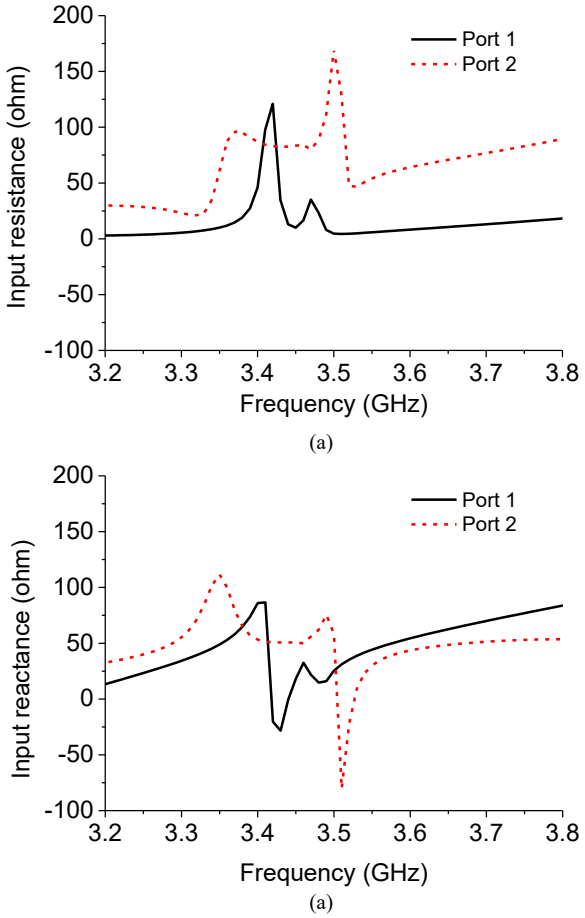

Fig. 5. Input (a) resistance and (b) reactance of the even-odd mode excited SSPPs.

Fig. 5 shows the input impedance of even-odd mode excited SSPPs. First as can be seen in Fig. 5 (a), when port 1 (even mode) is excited, there are two resonant resistance-peaks between 3.4 GHz and 3.5 GHz. While when port 2 (odd mode) is excited, there are three resonant resistance-peaks in the similar bandwidth. The flat and wide resistance curve for port 2 implies that the SSPPs under odd-mode excitation can have a low-Q resonance compared to the even-mode excitation. The curves in Fig. 5 (b) shows that the input reactances of the SSPPs under both two modes excitations are inductive. Therefore, there will be a challenge in matching the two modes in design of SSPP based antennas.

Fig. 6 gives the current distributions when port 1 and port 2 are excited respectively at 3.45 GHz. This further confirms the even-mode and odd-mode resonances are correctly excited through port 1 and port 2. First as can be seen in Fig. 6 (a), when port 1 is excited, even-mode current is overserved on the SSPPs with symmetrical distribution. While in Fig. 6 (b), symmetrical odd-mode current distribution is observed on the SSPPs. It can also be noticed that due to the close coupling from the bottom ground plane, the first SSPP unit cell has stronger current magnitude under both two excitations. This would be the possible reason of strong reactance under both even-mode and odd-mode resonances. Fig. 7 shows the respective 3D radiation patterns when port 1 and port 2 are excited. Owing the orthogonal even-mode and odd-mode current distributions on the SSPPs, orthogonal 3D radiation patterns are obtained as shown in Fig. 7 (a) and Fig. 7 (b). This shows the good patterns diversity of two different resonant mode.

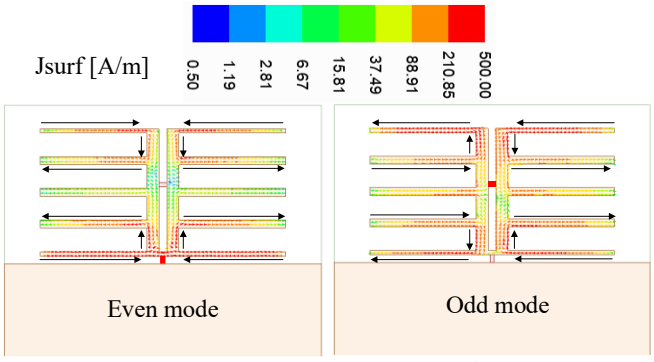

(a) (b)

Fig. 6. Current distribution on the even-odd mode excited SSPPs when (a) port 1 is excited and (b) port 2 is excited.

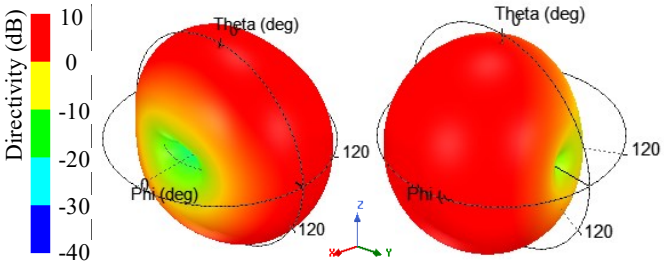

(a) (b)

Fig. 7. Simulated 3D radiation patterns of the even-odd mode excited SSPPs when (a) port 1 is excited and (b) port 2 is excited.

III. SSPPs-Based MIMO Antenna

Based on the above method to improve the consistency of the even-odd mode resonances on the SSPPs, SSPPs-based antenna element and its array are designed and developed for mobile terminal MIMO applications.

A. Element Design

Fig. 8 shows the configuration of the proposed SSPPs-based MIMO antenna element. As shown in Fig. 8 (a), the element is designed under a mobile phone platform using a common ground size of 150 mm×70 mm. The element is arranged at the center of the long side-edge to analyze its impedance and radiation performances. Both the mobile terminal ground platform and the antenna are printed on the low-cost FR4 substrate with the relative permittivity of 4.4 and thickness of 0.8 mm.

Fig. 8 (b) shows the detailed view of the antenna element. The copper of the antenna shown in the orange colour is printed on the back layer of the substrate, and the copper in green colour is printed on the front layer of the substrate. The even-mode radiation of the SSPPs is realized by exciting port 1 through a 50Ω microstrip line. Three conducting vias are used to connect the microstrip feedline to the back SSPPs. The odd-mode radiation of the SSPPs is realized by exciting port 2 through a coaxial cable. The outer conductor of the coaxial cable is soldered to the front copper of the antenna, while the inner conductor is penetrated through the substrate, and then soldered to the back copper of SSPPs. Note that the outer conductor of the coaxial cable at the other end is also connected to the ground plane for a stable performance in its input impedance. But the soldering distance (d1) is quite flexible and adjustable, as long as it is soldered to the main ground plane. The front copper is also connected to the back SSPPs through two vias for electrical connection.

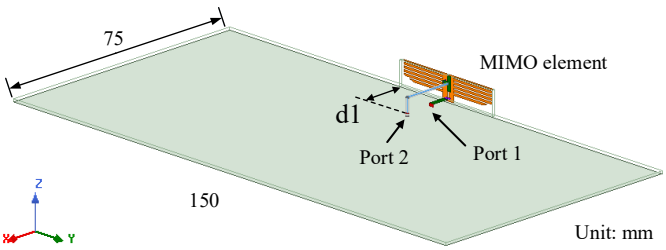

(a)

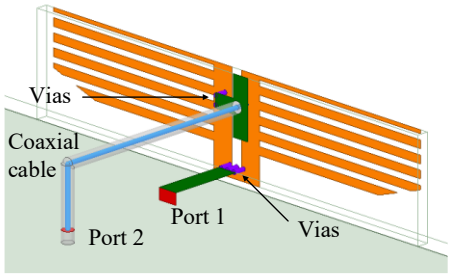

(b)

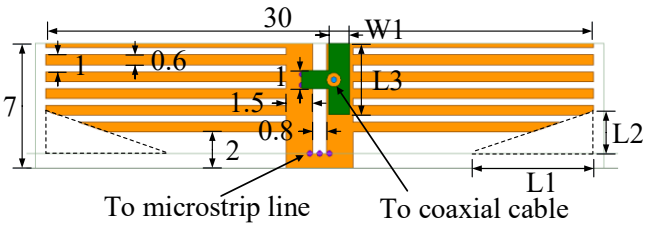

(c)

Fig. 8. Configuration of the designed SSPPs-based MIMO antenna element within a mobile phone platform. (a) 3D view, (b) enlarged view, and (c) top view. (Key design parameters in the figure, d1=15 mm, W1=1.2 mm, L1=6.4 mm, L2=2.4 mm, L3=4 mm.)

Fig. 8 (c) shows the top view of the designed SSPPs MIMO antenna, feed microstrip line and coaxial cable are hided for a better view. Five SSPP unit cells are utilized to excite the even-odd modes resonances. To get a better radiation for even-mode resonance and reduce the coupling from the reference ground plane, two symmetrical triangular cuts with

the lengths of L1 and L2 are removed from the SSPPs at the bottom. In addition, to get a better radiation efficiency for odd-mode resonance, the green patch with the width of W1 and length of L3 is introduced on the front layer for additional capacitance compensation.

Fig. 9 gives the simulated S-parameters of the designed SSPPs-based MIMO antenna element. It can be seen that a broad bandwidth is obtained at both two ports. The impedance bandwidth for S_{11}<-6 dB is 3.15-3.8 GHz, while the impedance bandwidth for S_{22}<-6 dB is 3.3-3.85 GHz. Because of the different quality factor in even-mode and odd-mode resonances, and also the asymmetrical effect of the reference ground plane, the bandwidths of two modes are different. The overlapped impedance bandwidth for both S_{11}<-6 dB and S_{22}<-6 dB is 3.3-3.8 GHz. Most importantly, because of the nature orthogonality of even-mode and odd-mode resonances, high isolation of more than 32.7 dB is obtained within the impedance bandwidth.

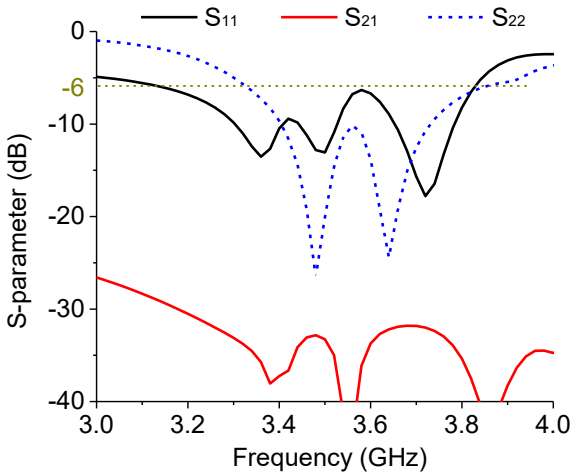

Fig. 9. Simulated S-parameters of the designed SSPPs-based MIMO antenna element.

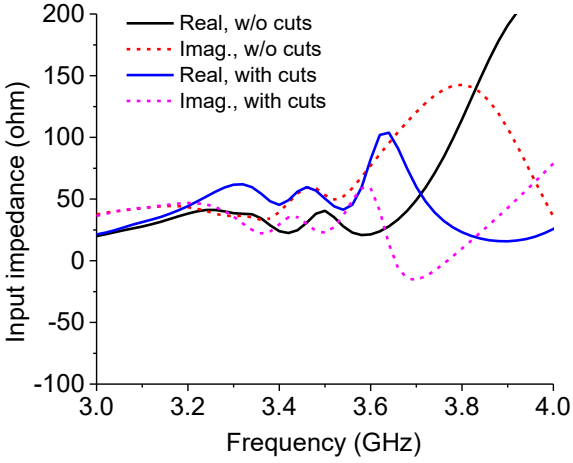

Fig. 10. Input impedance of port 1 for even-mode excitation when with and without the triangular cuts.

B. *Effect of the Triangular Cuts*

In the antenna element design, the symmetrical triangular cuts on the SSPPs are used to compensate the strong coupling between SSPPs and the reference ground plane. Fig. 10 shows the antenna input impedance when with and without the two triangular cuts. When without the cuts at the two corners, strong coupling from the ground plane causes the input resistance very low, with the average value close to 25Ω within the interested bandwidth. In addition, we can see the coupling is inductive, especially at the upper band-edge. To reduce the coupling effect from the ground plane, the triangular cuts at SSPPs corners are introduced. It can see that, the input resistance is increase substantially to around 50Ω, and the input reactance varies around zero at the upper bandwidth. Therefore, the input impedance bandwidth can be improved for the even-mode radiation on SSPPs.

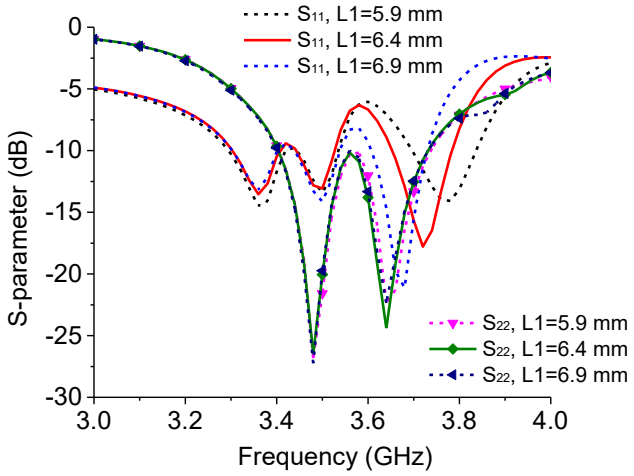

(a)

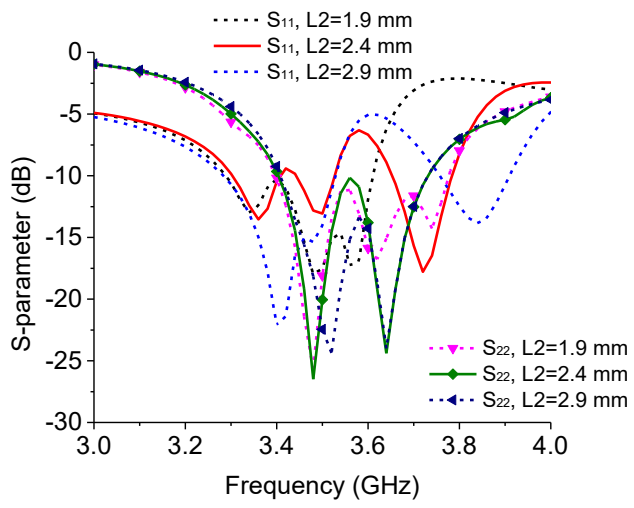

(b)

Fig. 11. S-parameters of the designed SSPPs MIMO antenna vary with the different (a) cut length L1 and (b) cut length L2.

Fig. 11 gives the detailed influences on the input impedance bandwidth from the triangular cuts in two-dimensional lengths L1 and L2. As shown in Fig. 11 (a), the change of L1 have a greatly effect on the bandwidth in the upper frequency band. As the increase of L1, the bandwidth shifts to upper frequency, which causes the reflection coefficient at the center slightly increased. The change of L1 has nearly no effect on the reflection coefficient of port 2, and the curves of S_{22} are almost overlapped. Compared to the effect of L1 in Fig. 11 (a), the effect of L2 in Fig. 11 (b) is more obvious, this is because that the variance of L2 will involve the cuts on the more or less

SSPP unit cells. Therefore as the change of L2, the reflection coefficient curve of S_{11} changes substantially at the upper band-edge, which causes the resulted bandwidth seriously reduced or increased. In addition, we can find L2 has a slight effect on the upper band-edge of port 2. This is because the length of the SSPP unit cells also has influence on the odd-mode resonance. From the two parameters, it can also be found that they have very slight effect on the lower frequency bandwidth. By tuning these two parameters, the upper frequency band can be effectively improved.

C. *Effect of the Capacitive Patch*

To get a good impedance matching for odd-mode radiation at port 2, the green copper patch connected to the outer conductor plays an important role in improving the impedance bandwidth. Fig. 12 shows the input impedance of port 2 when with and without the patch. It can be seen that when without the patch, the input impedance of SSPPs is inductive with the most of imaginary part greater than 0. Therefore, additional capacitance should be introduced to cancel this undesired inductance. A rectangular patch, which is equivalent as a capacitor, is connected to the outer conductor of the coaxial cable to improve the impedance bandwidth for port 2.

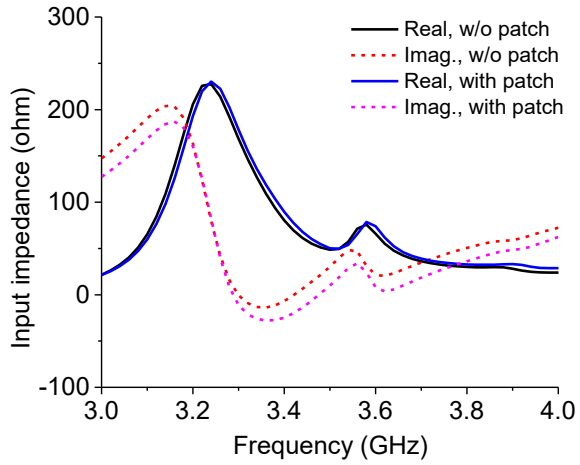

Fig. 12. Input impedance of port 2 for odd-mode excitation when with and without the patch.

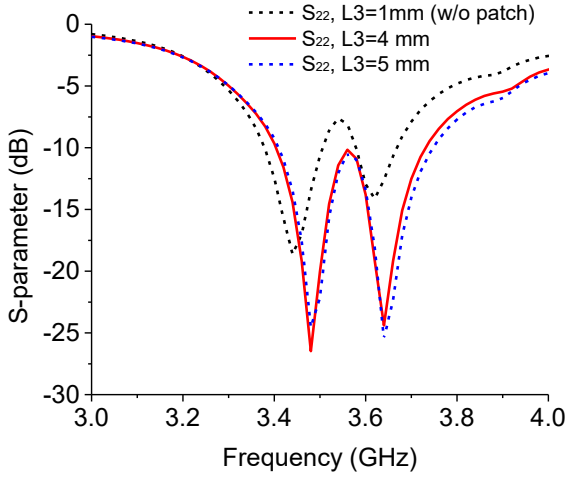

Fig. 13. S-parameters of the designed SSPPs MIMO antenna vary with the different patch length L3.

Fig. 13 shows the S-parameters changing with different lengths of the patch. Note that when L3=1 mm, it also means that no additional patch is connected to the outer conductor of the coaxial cable. As can be seen in the figure, the impedance bandwidth for port 2 can be improved by the introduced patch. As the increase of the length of the patch, more capacitance is compensated at port 2, and the impedance bandwidth of port 2 can be further improved.

D. *Effect of the Feed Coaxial Cable*

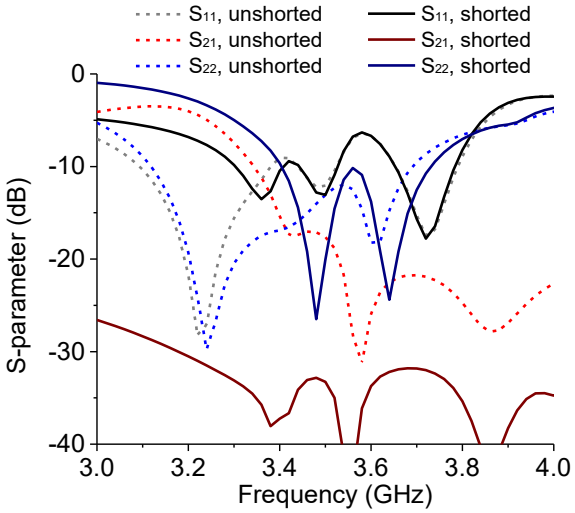

Fig. 14. S-parameters of the designed SSPPs MIMO antenna when the outer conductor of the coaxial cable is shorted or not shorted to the reference ground plane.

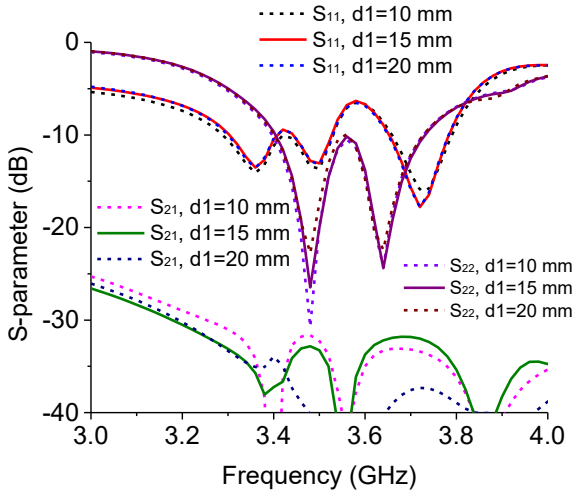

Fig. 15. S-parameters of the designed SSPPs MIMO antenna changing with different shorting distance d1 for port 2.

In the design of the SSPPs MIMO antenna element, one should be noted is that the shorting of the outer surface of the coaxial cable to the reference ground plane has a significant effect on the isolation performance. Fig. 14 shows the S-parameters of the designed antenna element when the outer conductor of the coaxial cable is shorted or not shorted to the reference ground plane. It can be seen that when the coaxial cable is not shorted to the ground, a poor isolation is obtained between the two ports. Although a much wider impedance bandwidth is achieved compared to the case of the shorted cable, the poor isolation denotes the unregulated wave will

transmit between two ports. The even-mode radiation and odd-mode radiation are not orthogonal with strong couplings. To get a high isolation between two driven ports and an excellent MIMO performance for the developed antenna, the outer conductor of the coaxial cable for port 2 should be connected to the reference ground plane.

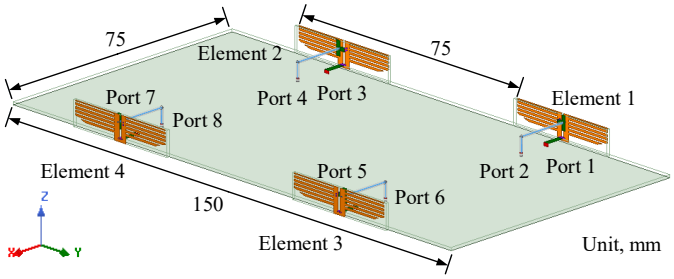

Fig. 16. Configuration of the designed SSPPs MIMO array antenna for mobile terminal applications.

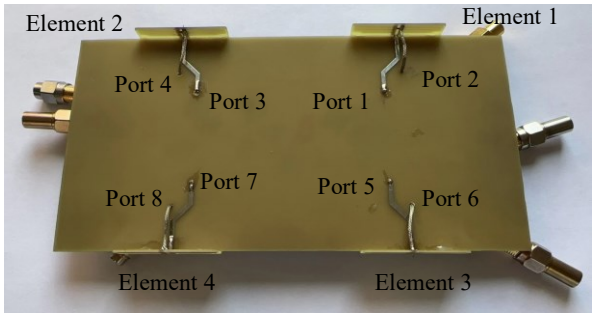

(a)

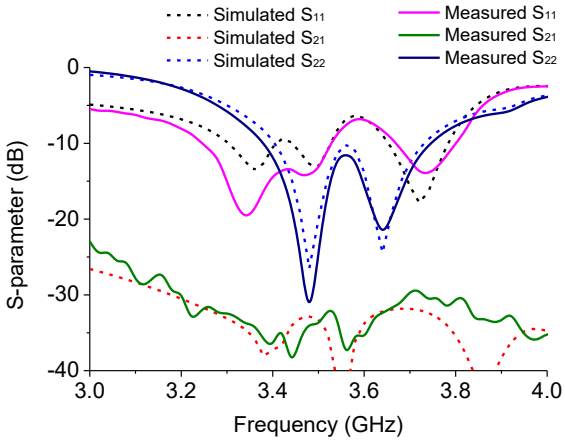

(b)

Fig. 17. (a) Photograph and (b) measured S-parameters of the fabricated prototype of the MIMO array antenna.

Because the shorting of the outer surface of the coaxial cable has an important role in improving the isolation of two driven ports, the question is will the S-parameters be changed with different shorting distances? This effect is studied and the results are shown in Fig. 15. It can be seen in the figure that, the shorting distance has nearly no effect on the S-parameters of the designed SSPPs-based MIMO antenna element, as long as the outer conductor of the coaxial cable is shorted to the reference ground plane. The reflection coefficient curves of two ports are nearly unchanged, and the coupling coefficients between two parts are well below -30 dB within the impedance bandwidth. Therefore, the coaxial cable can be connected quite freely as long as the outer conductor is connected to the reference ground plane.

E. Array Realization

Based on the SSPPs antenna element, an eight-port MIMO array antenna is developed, and its 3D view of the array configuration is shown in Fig. 16. As can be seen in the figure, four antenna elements are arranged at the two long-edges of the main circuit board with the distance of 75 mm. Each antenna element has the same configuration as the previously discussed element. The array antenna was then fabricated for further S-parameters and radiation patterns investigation at the University of Kent and Xidian University. Fig. 17 (a) shows the photograph of the fabricated array antenna prototype.

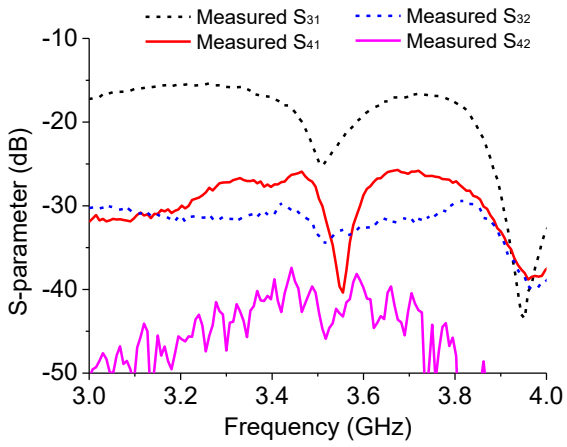

(a)

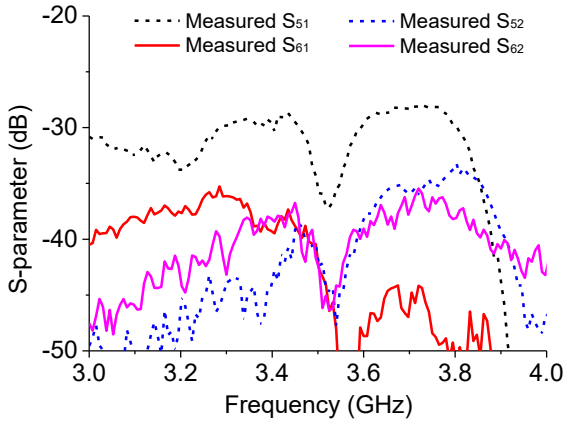

(b)

Fig. 18. Measured couplings of the fabricated MIMO array antenna. (a) Couplings between element-1 and element-2. (b) Couplings between element-1 and element-3

The measured S-parameters of the single SSPPs antenna element in the array are shown in Fig. 17 (b). Note that owing to the symmetry of the array structure, only S-parameters of one element are shown in the figure for brevity. The simulated results are also given in the figure for a good comparison. As can be seen, the measured impedance bandwidth for S_{11}<-6 dB is 3.08-3.84 GHz. The measured impedance bandwidth for S_{22}<-6 dB is 3.31-3.9 GHz. So the overlapped impedance bandwidth for two driven ports is 3.31-3.84 GHz. In addition, it can be found that a high isolation of over 29 dB is achieved

within the impedance bandwidth. Compared the simulated results, the measured results have a slight frequency band shift to the lower frequency.

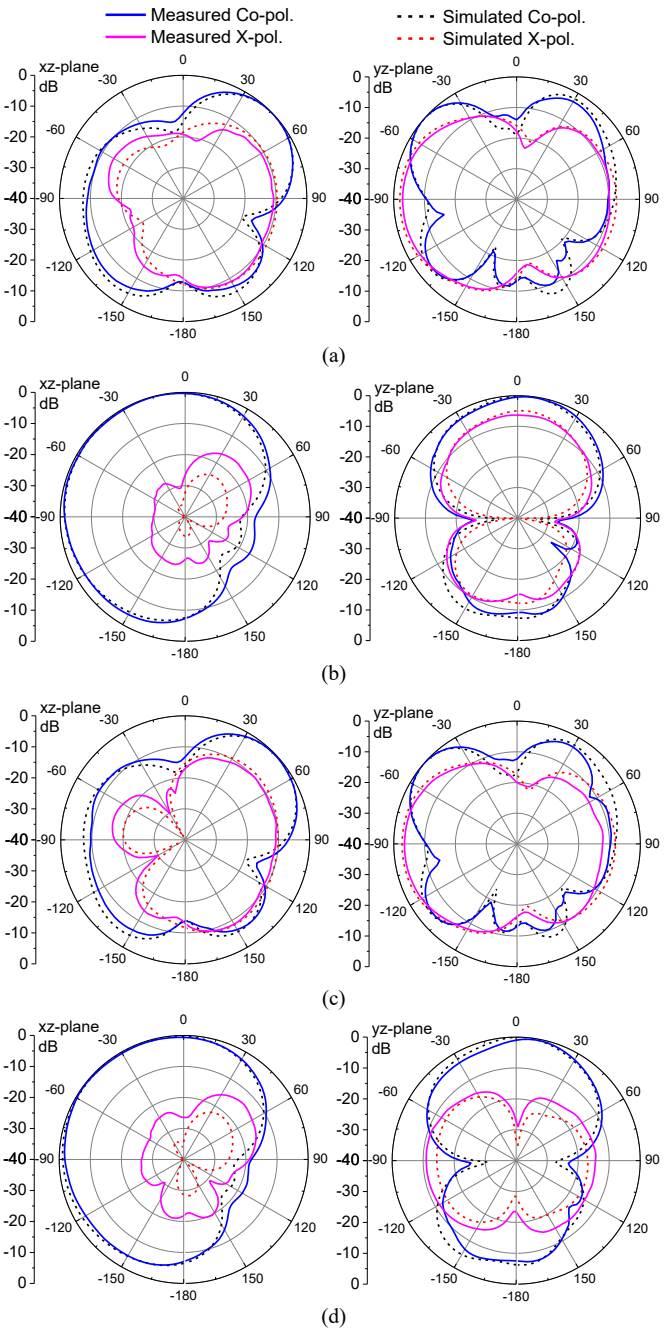

Fig. 19. Measured normalized radiation patterns of element-1 when (a) port 1 is excited at 3.4 GHz, (b) port 2 is excited at 3.4 GHz, (c) port 1 is excited at 3.7 GHz, and (d) port 2 is excited at 3.7 GHz.

The coupling between the adjacent elements are also investigated and shown in Fig. 18. Fig. 18 (a) shows the measured couplings between element-1 and element-2. As can be seen, the strong coupling is existed between port-1 and port-3, it is the coupling between the same even-mode radiations for different elements. The worst coupling is -15.6 dB in the working frequency band, which is good enough for mobile terminal MIMO applications. The coupling between other ports for element-1 and element-2 are quite weak and well below -25 dB. Fig. 18 (b) shows the measured couplings between element-1 and element-3. It can be seen that the coupling between two even-mode excited radiations is still stronger than the couplings between other ports. However, all these couplings are very weak, and lower than -28 dB.

Fig. 19 shows the measured normalized radiation patterns of element-1 at the different driven ports and in the different planes for the fabricated MIMO array antenna. It can be seen that, due to the different resonant modes at the different driven ports, the radiation patterns at the different ports are not similar. This will help to increase the patterns diversity for mobile terminals. In addition, it can be found that when driven by different ports, the maximum radiation directions are almost orthogonal. This will also be beneficial to improve the diversity of radiation patterns. Overall, compared to the simulated radiation patterns, the measured radiation patterns have a good agreement with the estimated results.

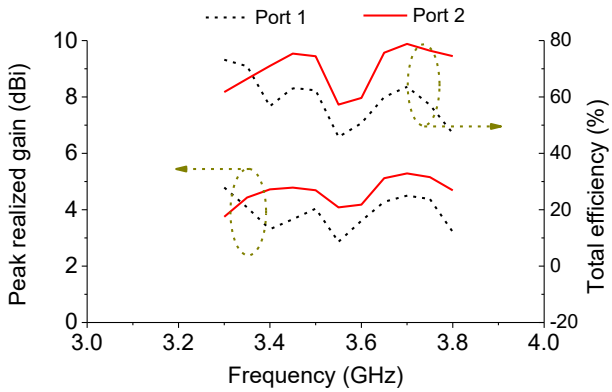

Fig. 20. Measured peak realized gains and total efficiencies of the element-1 in the MIMO array antenna.

TABLE I
COMPARISON OF THE RECENTLY PUBLISHED MIMO ANTENNAS

Ref.	Radiator Size ($\lambda_0\times\lambda_0$)	Thickness (λ_0)	BW (GHz)	RBW	Isolation	Efficiency
[22]	0.29×0.29	0.06	3.3-3.6	8.7%	>27 dB	N.G.
[23]	0.29×0.29	0.037	3.65-3.81	4.3%	>31 dB	N.G.
[24]	0.33×0.07	0.026	3.4-3.6	5.7%	>17.8 dB	59%-73%
[25]	0.32×0.32	0.019	3.3-3.8	14.1%	>20 dB	>40%
[26]	0.33×0.058	0.019	3.4-3.6	5.5%	>24 dB	>60%
This work	0.35×0.08	0.01	3.31-3.84	14.8%	>29 dB	60%-70%

Fig. 20 shows the measured peak realized gains and the total efficiencies of the elment-1 when driven by different ports. Note that the total efficiency is in consideration of the mismatch loss at the port, and it is calculated based on the measured peak realized gain and the directivity. As can be seen, although port-1 has a wider impedance bandwidth compared to the port-2, it has a relatively lower realized gain and lower total efficiency. This is perhaps due to the current cancellation when the antenna working in even-mode radiation. When the element-1 is working in even-mode radiation, the realized gain is around 4 dBi, and the total efficiency is around 60%. When the element is working in odd-mode radiation, the realized gain is around 4.5 dBi, and the total efficiency is around 70%.

Table I compares the performances of the proposed SSPPs based MIMO antenna with other recently developed MIMO antennas. Note that in the table, λ_0 is the freespace wavelength at the center operation frequency. We can see that the proposed MIMO antenna has a compact radiator size of $0.35\lambda_0 \times 0.08\lambda_0$ with a thin thickness of $0.01\lambda_0$ (0.8 mm). In a good comparison, a wide overlapped impedance bandwidth of 14.8% is achieved for this compact radiator size. Owing to the introduction of the natural orthogonality between the even-mode and odd-mode radiation, high isolation of 29 dB is obtained for the developed MIMO element. Therefore, observing the performance comparison in the table, the proposed SSPPs based antenna element and its array can be good candidates for mobile terminal applications.

IV. Conclusion

This paper presents the works on the SSPPs based compact antenna and array for MIMO applications by using even and odd mode resonances. A new SSPPs structure composed of corrugated grooves with a dedicated separate distance is proposed with consistent even and odd mode resonances. Therefore, SSPPs can have resonances in the same working frequency band. In addition, even and odd mode radiations are successfully and respectively excited at the same SSPPs aperture using the developed driven methods. Due to the difference in the resonance modes, challenges of impedance matching at two driven ports are overcome by introducing the capacitive patch and triangular cuts on the SSPPs structure. Finally, the compact SSPPs based element and array were developed for MIMO applications. Both the measured and simulated results prove that the element can have a wide impedance bandwidth of 3.31-3.84 GHz with a high isolation of 29 dB. The low couplings between antenna elements, diversified radiation patterns, high realized gain, and radiation efficiency show that the designed SSPPs array antenna can be a good candidate for MIMO applications.

References

[1] J. B. Pendry, L. Martín-Moreno and F. J. Garcia-Vidal, "Mimicking surface plasmons with structured surfaces", *Science*, vol. 305, pp. 847-848, Aug. 2004.

[2] D. -Y. Li, Y. -C. Jiao, H. -W. Yu and Z. -B. Weng, "Wideband circularly polarized pyramidal horn antenna based on spoof surface plasmon polaritons," *IEEE Trans. Antennas Propag.*, vol. 69, no. 4, pp. 2353-2358, April 2021.

[3] B. Xu, Z. Li, L. Liu, J. Xu, C. Chen, P. Ning, X. Chen, and C. Gu, "Tunable band-notched coplanar waveguide based on localized spoof surface plasmons," *Opt. Lett.* vol. 40, no. 20, pp. 4683-4686 Oct. 2015.

[4] Z. -B. Yang et al., "Low-loss spoof surface plasmon polariton based on folded substrate integrated waveguide," *IEEE Antennas Wireless Propag. Lett.*, vol. 18, no. 1, pp. 222-225, Jan. 2019.

[5] Mark A. Cappelli, Hossein Mehrpour Bernety, Daniel Sun, Luc Houriez, and Benjamin Wang, "Tunable non-reciprocal waveguide using spoof plasmon polariton coupling to a gaseous magnetoplasmon," *Opt. Lett.*, vol. 48, no. 14, pp. 3725-3728, July 2023.

[6] H. Zhu, Y. Zhang, L. Ye, Z. Dang, R. Xu and B. Yan, "High-efficiency excitation of spoof surface plasmon polaritons through rectangular waveguide using dipole antenna," *IEEE Trans. Antennas Propag.*, vol. 70, no. 5, pp. 3899-3903, May 2022.

[7] E. Farokhipour, N. Komjani, M. A. Chaychizadeh, "An ultra-wideband three-way power divider based on spoof surface plasmon polaritons," *J. Appl. Phys.*, vol. 124, no. 23, pp. 235310, Dec. 2018.

[8] S. Mirhadi and N. Komjani, "A dual-band power divider based on higher-order modes of spoof surface plasmon polaritons," *AIP Adv.,* vol. 11, no. 9, pp. 095102, Sept. 2021.

[9] X. Yang, J.Luo, D. Gu, P. Su, M. Zhang, Z. Zhu, and J. Yuan, "High-efficiency electrically direction-controllable spoof surface plasmon polaritons coupler," *J. Appl. Phys.,* vol. 127 no. 23, pp. 233105, June 2020.

[10] L. Liu and D. Jiang, "A microwave detector based on spoof surface plasmon polaritons structure," *AIP Adv.*, vol. 11 no. 3, pp. 035008, Mar. 2021.

[11] Xiang-Jun Li, et al., "One-dimensional terahertz dielectric gradient metasurface for broadband spoof surface plasmon polaritons couplers," *Opt. Lett.,* vol. 46, no. 2, pp. 290-293, Jan. 2021.

[12] Y. Pang, Y. Li, J. Zhang, Z. Xu and S. Qu, "Design of frequency selective surface based on spoof surface plasmon polariton modes," *IEEE Antennas Wireless Propag. Lett.*, vol. 17, no. 6, pp. 1123-1126, June 2018.

[13] E. Klopfer, H. Carr Delgado, S. Dagli, Mark Lawrence, Jennifer A. Dionne, "A thermally controlled high-Q metasurface lens," *Appl. Phys. Lett.*, vol. 122, no. 22, pp. 22170129, May 2023.

[14] H. Zhao, F. Ge, Q. Zhang, S. Li and X. Yin, "Asymmetric endfire frequency scanning tapered slot antenna with spoof surface plasmon polaritons," *IEEE Trans. Antennas Propag.*, vol. 70, no. 7, pp. 5913-5917, July 2022.

[15] C. Zhang, J. Ren, X. Du and Y. Yin, "Dual-beam leaky-wave antenna based on dual-mode spoof surface plasmon polaritons," *IEEE Antennas Wireless Propag. Lett.*, vol. 20, no. 10, pp. 2008-2012, Oct. 2021.

[16] Q. Zhang, Q. Zhang and Y. Chen, "Spoof surface plasmon polariton leaky-wave antennas using periodically loaded patches above PEC and AMC ground planes," *IEEE Antennas Wireless Propag. Lett.*, vol. 16, pp. 3014-3017, 2017.

[17] J.Y. Yin, et al., "Endfire radiations of spoof surface plasmon polaritons," *IEEE Antennas Wireless Propag. Lett.,* vol. 16, pp. 597-600, 2017.

[18] X. Du, H. Li and Y. Yin, "Wideband fish-bone antenna utilizing odd-mode spoof surface plasmon polaritons for endfire radiation," *IEEE Trans. Antennas Propag.*, vol. 67, no. 7, pp. 4848-4853, July 2019.

[19] D.-Y. Li, Y.-C. Jiao, H.-W. Yu and Z.-B. Weng, "Wideband circularly polarized pyramidal horn antenna based on spoof surface plasmon polaritons," *IEEE Trans. Antennas Propag.*, vol. 69, no. 4, pp. 2353-2358, April 2021.

[20] H. Li, X. Du, T. Feng, L. Wen and Y. Yin, "Circularly polarized antenna with spoof surface plasmon polaritons transmission lines," *IEEE Antennas Wireless Propag. Lett.*, vol. 18, no. 4, pp. 737-741, April 2019.

[21] M. Hasan, İ. Bahçeci and B. A. Cetiner, "Downlink multi-user MIMO transmission for radiation pattern reconfigurable antenna systems," *IEEE Trans. Wireless Commun.*, vol. 17, no. 10, pp. 6448-6463, Oct. 2018.

[22] H. Huang, X. Li and Y. Liu, "A low-profile, dual-polarized patch antenna for 5G MIMO application," *IEEE Trans. Antennas Propag.,* vol. 67, no. 2, pp. 1275-1279, Feb. 2019.

[23] Y. Gao, R. Ma, Y. Wang, Q. Zhang and C. Parini, "Stacked patch antenna with dual-polarization and low mutual coupling for massive MIMO," *IEEE Trans. Antennas Propag.,* vol. 64, no. 10, pp. 4544-4549, Oct. 2016.

[24] A. Ren, Y. Liu and C. Sim, "A compact building block with two shared-aperture antennas for eight-antenna MIMO array in metal-rimmed smartphone," *IEEE Trans. Antennas Propag.*, vol. 67, no. 10, pp. 6430-6438, Oct. 2019.

[25] W. Hu et al., "Wideband back-cover antenna design using dual characteristic modes with high isolation for 5G MIMO smartphone," *IEEE Trans. Antennas Propag.*, vol. 70, no. 7, pp. 5254-5265, July 2022.

[26] H. Xu, S. S. Gao, H. Zhou, H. Wang and Y. Cheng, "A highly integrated MIMO antenna unit: differential/common mode design," *IEEE Trans. Antennas Propag.,* vol. 67, no. 11, pp. 6724-6734, Nov. 2019.

[27] P.H. He, L.Y. Niu, Y. Fan, H.C. Zhang, L.P. Zhang, et al. "Active odd-mode-metachannel for single-conductor systems," *Opto-Electron Adv*. vol. 5, no. 8, 210119, Aug. 2022.

[28] L.Y. Niu, P.H. He, Y. Fan, L.P. Zhang, H. C. Zhang, T.J. Cui, "Gain-associated nonlinear phenomenon in single-conductor odd-mode plasmonic metamaterials," *Laser Photonics Rev.,* vol. 16, no. 6, 2100619, June 2022.

Lehu Wen (Senior Member, IEEE) received Ph.D. degree in Electronic Engineering from the University of Kent, Canterbury, U.K., in 2020.

From 11/2020 to 02/2023, he was Research Fellow with the School of Engineering, University of Kent, Canterbury, U.K. From 03/2023 to 09/2023, he was Research Fellow with the Department of Electronic and Electrical Engineering, University College London, U.K. He is currently a Lecturer with the Department of Electronic and Electrical Engineering, Brunel University London, U.K. His research interests include wideband Reflectarray, Transmitarray, dual-polarized antennas, circularly polarized antennas, tightly coupled array antennas, and mobile terminal antennas.

He received the Best Student Paper Award in ISAP2019 and 1/10 Best Conference Paper in iWAT 2022. He presented the invited talks on dual-polarized antennas in CAMA 2021 and APMC 2020. He was a Track Chair in IEEE ISAP 2022 and a Session Chair in EMW 2021. He serves as a regular Reviewer for journals of IEEE Transactions on Antennas and Propagation, IEEE Antennas and Wireless Propagation Letters, International Journal of RF and Microwave Computer-Aided Engineering, etc. He was an Exceptional Reviewer of IEEE Transactions on Antennas and Propagation in 2021.

Wei Hu (Senior Member, IEEE) received the Ph.D. degree in electromagnetic fields and microwave technology from Xidian University, Xi'an, China, in 2013.

From 2013 to 2017, he was a Lecturer with the National Key Laboratory of Antennas and Microwave Technology, Collaborative Innovation Center of Information Sensing and Understanding, Xidian University, where he is currently an Associate Professor. From 2018 to 2019, he was an Academic Visitor with the University of Kent, Kent, U.K.

He has authored or coauthored over 80 internationally refereed journal articles and has been serving as a reviewer for a number of technical journals and international conferences. His current research interests include multiband and wideband antennas, circularly polarized antennas, multiple-input multiple-output antenna arrays, and wideband wide-scanning phased arrays.

Bo Pang received the B.S. degree in electronic science and technology from the Guilin University of Electronic Technology, Guilin, China, in 2016. He is currently pursuing the Ph.D. degree in electromagnetic wave and microwave technology with Xidian University, Xi'an, China.

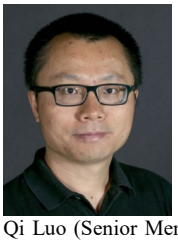

Qi Luo (Senior Member, IEEE) received the M.Sc. degree (Hons.) from the University of Sheffield, Sheffield, U.K., in 2006, and the Ph.D. degree (Hons.) from the University of Porto, Porto, Portugal, in 2012.

From 2012 to 2013, he was a Research Fellow with the Surrey Space Center, Guildford, U.K. From 2013 to 2020, he was a Research Fellow with the School of Engineering and Digital Arts, University of Kent, Canterbury, U.K. He is currently a Reader with the Department of Engineering and Technology, University of Hertfordshire, Hatfield, U.K.

He has authored or co-authored two books Circularly Polarized Antennas (Wiley–IEEE, 2014) and Low-Cost Smart Antennas (Wiley, 2019). He also authored a book chapter in Handbook of Antenna Technologies (Singapore: Springer, 2014). His current research interests include smart antennas, circularly polarized antennas, reflectarray, transmitarray, multiband microstrip antennas, and electrically small antenna design.

Steven Gao (Fellow IEEE) received the Ph.D. degree in microwave engineering from Shanghai University, Shanghai, China, in 1999.

Steven Gao is currently a Professor at the Chinese University of Hong Kong, and an Honorary Professor at the University of Kent, UK. He coauthored/co-edited three books, such as Space Antenna Handbook (Wiley, 2012), Circularly Polarized Antennas (IEEE–Wiley, 2014), and LowCost Smart Antennas (Wiley, 2019), over 300 papers, and ten patents. His research interests include smart antennas, phased arrays, multiple-input multiple-output, reconfigurable antennas, wideband multiband antennas, satellite antennas, RF microwave mmWave THz circuits, mobile communications, satellite communications, ultrawideband radars, syntheticaperture radars, the IoT, and sensors for healthcare.

He is a Fellow of the Royal Aeronautical Society, U.K., and the IET, U.K. He was a Distinguished Lecturer of the IEEE AP Society. He was the General Chair of the Loughborough Antennas and Propagation Conference (LAPC) 2013 and an invited speaker at many conferences. He is currently an Associate Editor of several other international journals, including IEEE Transactions on Antennas and Propagation, Radio Science, IEEE Access, Electronics Letters, and IET Circuits, Devices and Systems, and the Editorin-Chief for John Wiley & Sons Book Series on Microwave and Wireless Technologies. He was Associate Editor of IEEE Transactions on Antennas and Propagation (2015-2021). He is currently the Editor-in-Chief of IEEE Antennas and Wireless Propagation Letters.